

The in situ origin of the globular cluster NGC 6388 from abundances of Sc, V, and Zn of a large sample of stars[★]

Eugenio Carretta¹ and Angela Bragaglia¹

INAF-Osservatorio di Astrofisica e Scienza dello Spazio di Bologna, via Gobetti 93/3, I-40129 Bologna, Italy

ABSTRACT

Chemical tagging of globular clusters (GCs) is often done using abundances of α -elements. The iron-peak elements Sc, V, and in particular Zn were proposed as an alternative to α -elements to tag accreted GCs in the metal-rich regime, where the dwarf galaxy Sagittarius and its GCs show peculiarly marked under-abundances of these heavier species with respect to Milky Way stars. A handful of stars in NGC 6388 was used to suggest an accreted origin for this GC, contradicting the results from dynamics. We tested the efficiency of the iron-peak method by using large samples of stars in NGC 6388, compared to thousands of field stars in the disc and the bulge of the Milky Way. Our abundance ratios of Sc (185 stars) and V (35 stars) for NGC 6388 are within about 1.5σ from the average for the field stars with a similar metallicity, and they are in perfect agreement for Zn (31 stars), claimed to be the most sensitive element concerning the accretion pattern. Moreover, the chemo-dynamical plots, coupled to the bifurcated age-metallicity relation of GCs in the Galaxy, clearly rule out any association of NGC 6388 to the groups of accreted GCs. Using a large set of GC abundances from the literature, we also show that the new method with Sc, V, and Zn seems to be efficient in picking up GCs related to the Sagittarius dwarf galaxy. Whether this is also generally true for accreted GCs seems to be less evident, and it should be verified with larger and homogeneous samples of stars both in the field and in GCs.

Key words. Stars: abundances – Galaxy: kinematics and dynamics – Galaxy: formation – Galaxy: globular clusters – Galaxy: globular clusters: individual: NGC 6388

1. Introduction

Using chemical abundances to tag the origin of stellar systems (see Freeman and Bland-Hawthorn 2002) is a challenging task. Yet, many elements and their combinations have been successfully used to separate the main populations (halo, bulge, and thin and thick disc) and the accreted substructures of the Milky Way (MW; e.g. Nissen and Schuster 2010, Hasselquist et al. 2019, Feuillet et al. 2021). Minelli et al. (2021a: M21a) recently proposed using the iron-peak elements Sc, V, and Zn to explore the metal-rich ($[\text{Fe}/\text{H}] \gtrsim -1$ dex) regime since they observed large differences in the abundances between stars in the MW and those in the Large Magellanic Cloud (LMC), as well as in the Sagittarius dwarf spheroidal galaxy (Sag) in this metallicity range. In Minelli et al. (2021b: M21b) they compared a handful of stars homogeneously analysed in four metal-rich globular clusters (GCs), concluding that NGC 5927 and NGC 6496 are formed in situ, whereas NGC 6388 and NGC 6441 are probably accreted, which is at variance with the classification of NGC 6388 in Massari et al. (2019) and Forbes (2020) but in agreement with Horta et al. (2020).

Given this controversial attribution, we decided to re-examine the origin of NGC 6388 by using much larger and statistically robust samples, both of the cluster and the comparison stars in the Galactic environment. In addition, new insights as to this issue may be gained by using not only four GCs, but all the clusters for which homogeneous integral of motion (IOM), orbital parameters, and chemical information are available.

Samples, data, and our analysis are briefly described in Section 2, and our results are presented in Section 3. The chemo-dynamics of the whole Galactic system of GCs is used in Section 4 to better assess the probable origin of NGC 6388, testing the ability of iron-peak elements to pick up accreted GCs in general, or only those with the peculiar chemical pattern typical of the Sag dwarf.

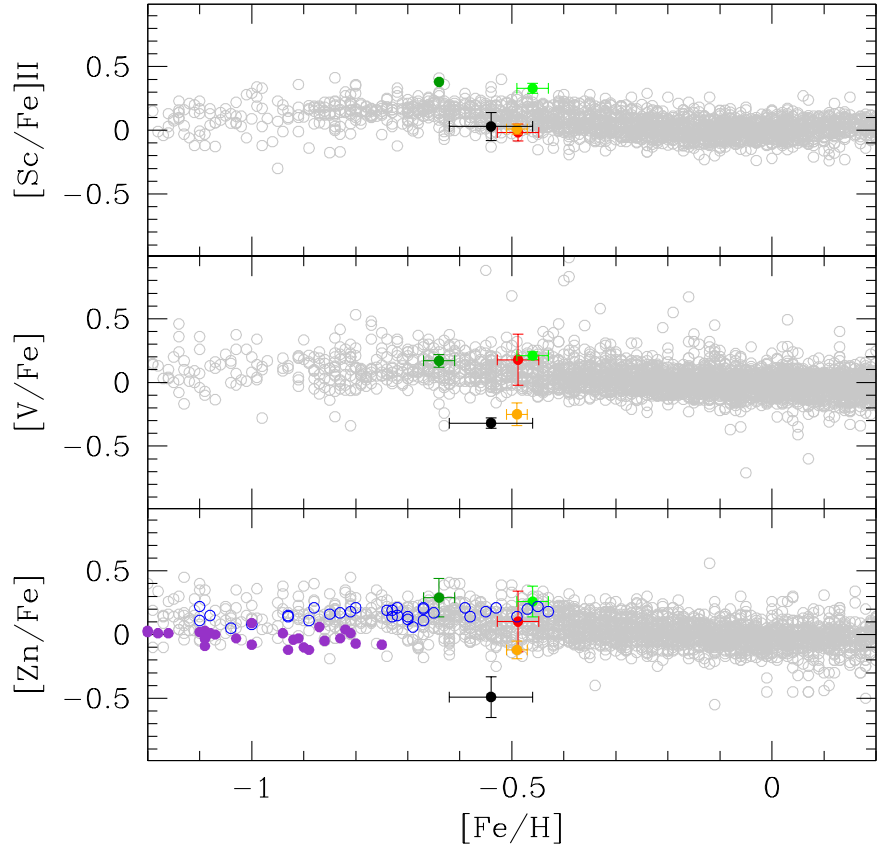
2. The data set

The data are those from our project on NGC 6388 ‘re-loaded’, where we exploited the richness of spectra in the ESO archive to assemble a data set of 185 highly probable members in this GC, heavily contaminated by bulge stars. They were analysed exactly as in our FLAMES survey (see e.g. Carretta et al. 2006 and Carretta et al. 2010a) and are based on high resolution UVES spectra or GIRAFFE HR13 spectra. Line lists, solar reference abundances, and corrections for a hyperfine structure for Sc and V are from Gratton et al. (2003).

Send offprint requests to: E. Carretta, eugenio.carretta@inaf.it

[★] Based on observations collected at ESO telescopes under programmes 073.D-0211, 073.D-0760, 381.D-0329, 095.D-0834, and 099.D-0047.

Fig. 1. Mean abundance ratios and rms scatters for $[\text{Sc}/\text{Fe}]$, $[\text{V}/\text{Fe}]$, and $[\text{Zn}/\text{Fe}]$ in NGC 6388 from the present study (red points with errorbars) and in NGC 6388 (orange points), NGC 6441 (black points), NGC 5927 (light green points), and NGC 6496 (dark green points) from Minelli et al. (2021b). Empty grey circles are field disc and bulge stars from Adibekyan et al. (2012), Battistini and Bensby (2015), Bensby et al. (2005, 2014, 2017), Bihain et al. (2004), Brewer et al. (2016), da Silva et al. (2018), Delgado-Mena et al. (2017), Gratton et al. (2003), Ishigaki et al. (2012, 2013), Lomaeva et al. (2019), Lucey et al. (2019), and Reddy et al. (2003, 2006). Open blue circles and filled violet circles are the high- α and low- α stars in the local sample by Nissen and Schuster (2011).



Atmospheric parameters and metallicities for the whole sample were presented in Carretta and Bragaglia (2021a). Individual abundances of Sc, V, and Zn from archival UVES spectra were partly shown in Carretta and Bragaglia (2018). These data are complemented by abundances for individual stars from our newly acquired UVES (12 stars) and GIRAFFE HR13 spectra (150 stars). All the data not shown in Carretta and Bragaglia (2018) will be presented and discussed in the final paper of this series, mainly devoted to the properties of multiple stellar populations in NGC 6388.

The abundances were derived using equivalent widths (EWs). Those measured in GIRAFFE spectra were shifted to the system of UVES EWs using stars observed with both spectrographs (Carretta and Bragaglia, in prep.). In total, our samples for the present work include 185 stars with a Sc abundance from UVES and GIRAFFE spectra, 35 stars with a V abundance, and 31 stars with a Zn abundance. The resulting mean abundance ratios are $[\text{Sc}/\text{Fe}] = -0.02$ dex (rms=0.07 dex), $[\text{V}/\text{Fe}] = +0.26$ dex (rms=0.14 dex), and $[\text{Zn}/\text{Fe}] = +0.10$ dex (rms=0.24 dex).

On average, abundances of Sc were obtained from eight lines for UVES spectra and two lines for GIRAFFE spectra. Abundances of V and Zn, which are only available for stars with UVES spectra, were derived from 12 lines and only one line (Zn λ 4810.54 Å), respectively. Internal errors, estimated with our usual procedure (see the Appendices in Carretta et al. 2009a,b), are 0.074 dex and 0.088 dex for Sc (for UVES and

GIRAFFE, respectively), 0.074 dex for V, and 0.190 dex for Zn (only one transition available). There is no trend as a function of the effective temperature in any of the element abundances.

A detailed comparison of abundances in NGC 6388 is only feasible for Zn, since we in addition to M21b used the same line. Taking differences into account due to the adopted solar reference abundances and the scale of atmospheric parameters, the final $[\text{Zn}/\text{Fe}]$ ratios would be virtually the same in the two analyses (see Appendix A).

The Sc abundances were already used in Carretta and Bragaglia (2019) to define a robust upper limit to the inner temperature reached by the putative polluters of the first generation (FG) stars in NGC 6388, that is those that likely enriched the proto-cluster environment in products of the proton-capture reactions in H-burning at a very high temperature (see the review by Gratton et al. 2019). When we compared the abundances of Mg and Sc for 185 stars in NGC 6388 to the pattern of field stars from Gratton et al. (2003), we found that the distribution of cluster stars was an almost perfect match to the field stars (Carretta and Bragaglia 2019). While providing strong constraints on the physical properties of FG polluters in NGC 6388, the above comparison implicitly showed that no significant difference was found between the cluster and field stars for one of the three species claimed by M21a to be a good indicator of nucleosynthesis associated to extragalactic and/or accreted objects.

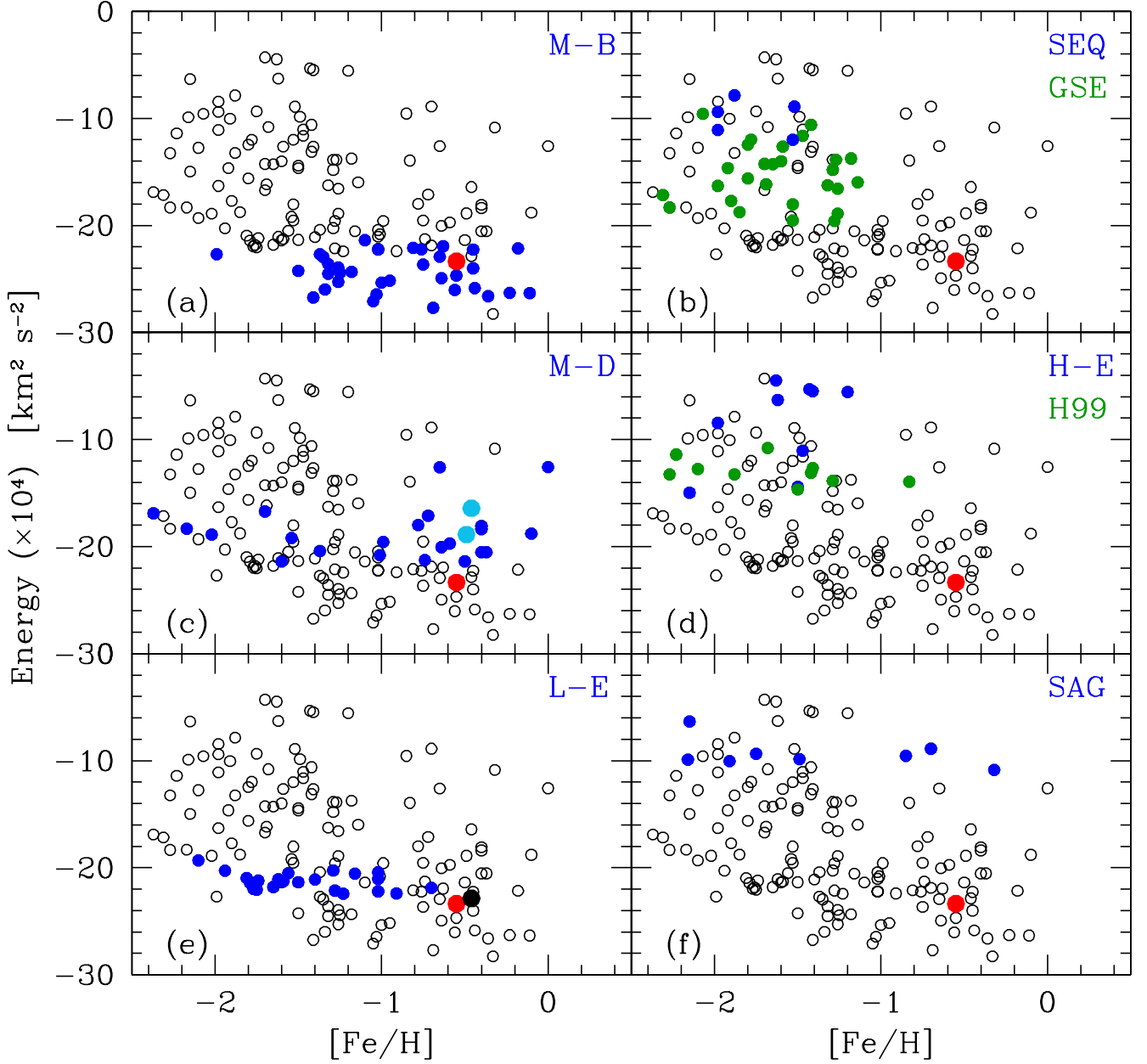


Fig. 2. Orbital energy E as a function of the metallicity $[Fe/H]$ for 147 GCs (empty circles) with orbital parameters from Savino and Posti (2019) and a kinematical classification in Massari et al. (2019). The different panels show the position of NGC 6388 (red filled circle), NGC 6441 (black filled circle, panel (e)), and NGC 5927 and NGC 6496 (cyan circles, panel (c)). In each panel, GCs associated to different merger events or those that formed in situ (Massari et al. 2019) are also indicated. The acronyms have the following meanings: main bulge (M-B), main disc (M-D), low energy (L-E), Sequoia (SEQ), Gaia-Sausage-Enceladus (GSE), high energy (H-E), Helmi streams (H99), and Sagittarius (SAG).

3. Results

In Carretta and Bragaglia (2019) we only compared the Sc pattern with the sample of field stars by Gratton et al. (2003). To better ascertain the membership of NGC 6388 to the autochthonous stellar populations of the MW, in Fig. 1 (upper panel), we compare the average $[Sc/Fe]$ abundance measured

from 185 cluster stars to different abundance analyses of field stars both in the Galactic disc (the majority of samples) and the Galactic bulge, in the metallicity range from $[Fe/H] = -1.2$ dex to 0.2 dex, centred on the mean metal abundance of NGC 6388. As also stated by M21b, the abundance ratios of iron-peak elements of disc and bulge stars are nearly identical (see also

Griffith et al. 2021). The comparison is extended to V and Zn abundances in the middle and lower panels, respectively. In each panel, the mean values and rms scatters from M21b are also indicated for reference.

Considering the intrinsic dispersion associated to the mean values, there is no evidence of a significant difference between NGC 6388 (red and orange circles in Fig. 1 correspond to our study and that of M21b, respectively) and field stars for Sc. Even NGC 6441 (M21b, black circle) agrees with the pattern of field stars; whereas, for NGC 5927 and NGC 6496 (the GCs of in situ origin), the Sc seems to be overabundant with respect to the field stars, although still roughly compatible with the field distribution.

For V, our value based on 35 stars lies inside the field star distribution at the same level of the mean values for NGC 5927 and NGC 6496. NGC 6441 (two stars) and NGC 6388 (four stars) from M21b lie below the field star distribution.

Concerning the Zn abundance, all the mean values for the GCs are in good agreement with the pattern defined by field disc and bulge stars of the Galaxy, except for NGC 6441 from M21b. We would like to caution readers that the results for NGC 6441 – in particular those for Zn, resting on a single line lying very close to the blue spectrum border of the lower signal-to-noise ratio (S/N) – could be affected by a S/N lower than optimal, as only about a third of the requested observations were actually obtained (see Carretta and Bragaglia 2021b).

In summary, our [Sc/Fe] ratio lies at the lower end of the distribution of field stars with a metallicity similar to that of NGC 6388, while the V abundance is close to the upper end. However, both values are compatible with the field stars' distribution; in terms of the standard deviation, neither exceeds 1.7σ from the disc/bulge mean value centred on the metallicity of NGC 6388. On the other hand, for Zn, which is claimed to be the most sensitive indicator of the accretion's chemical pattern (M21a,b), our average [Zn/Fe] ratio is in perfect agreement with the bulk of stars in the Galaxy.

Moreover, in many analyses of disc/bulge stars that we used as a comparison, no star is present in the low-Zn region around [Zn/Fe] ~ -0.5 dex. Were an accreted galaxy to produce a set of GCs with such a low Zn level, we would also expect the presence of debris consisting of accreted field stars with a similarly low Zn pattern, which are not observed here. Stars in the MW actually do reach such a low Zn content, but they are bona fide bulge stars, which are exclusively confined at a metallicity around and above [Fe/H] = 0.0 dex (da Silva et al. 2018), and more than 0.5 dex higher than the metallicity of NGC 6388 or the Sag and LMC stars observed in M21a. The low- α stars in the solar vicinity by Nissen and Schuster (2011) reach a plateau of [Zn/Fe] ~ -0.030 dex (rms=0.057 dex) above [Fe/H] > -1.1 dex (see Fig. 1). However, the absence of evidence is not evidence of an absence, and perhaps we are seeing a void simply due to uncomplete or unfortunate sampling of Galactic populations. In any case, the results of our analysis seem to exclude an accreted origin for NGC 6388.

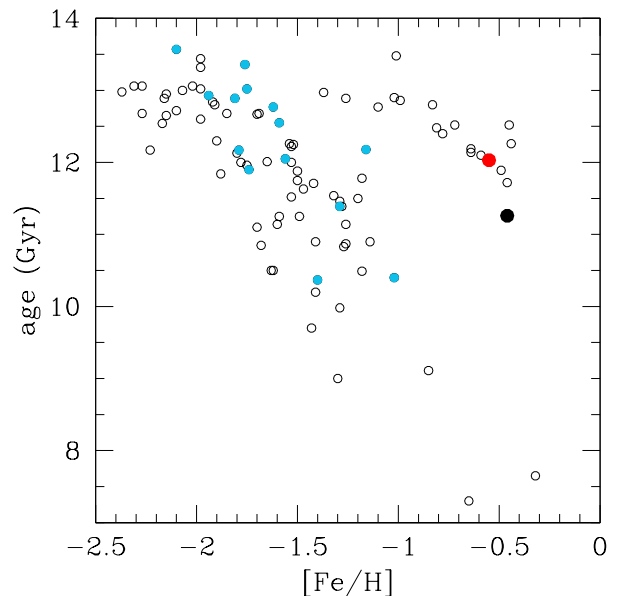


Fig. 3. Age-metallicity relation for a sample of GCs with an age from Kruijssen et al. (2019). We highlight the L-E GCs in Massari et al. (2019) as filled light blue points, NGC 6388 (red point), and NGC 6441 (black point).

4. Discussion and conclusions

Our abundance analysis of Sc, V, and Zn abundances for a relevant number of stars in NGC 6388 shows a chemical pattern virtually indistinguishable from that of field disc and bulge stars of our Galaxy at a similar metallicity. We anticipate that also the average [Si/Fe] (~ 0.30 dex from 184 stars, Carretta and Bragaglia, in prep.) supports the in situ formation of NGC 6388, which is in disagreement with the conclusion by Horta et al. (2020), who assign it to Sequoia. Their association was made on the basis of the Si abundance of a smaller number of stars (24, but with only six meeting the quality criteria defined by Mészáros et al. 2020) in the infrared data by APOGEE.

To help discriminate between different conclusions about the ancestral origin of NGC 6388, we used the chemodynamical plane shown in Fig. 2. We plotted the orbital energy E from Savino and Posti (2019; we verified that the results did not change using the set by Massari et al. 2019) as a function of the metallicity of the GCs from Harris (1996, using the 2010 online edition, which adopts the metallicity scale defined in Carretta et al. 2009c). Since the integrals of motion such as the orbital energy remain constant along an orbit, the clumping of GCs around a given energy level may indicate that they share(d) common orbital paths and likely had the same origin in a common ancestral system. This is basically the observation used by Massari et al. (2019), Forbes (2020), Myeong et al. (2019), among others to pick up coherent ensembles of GCs associated to past merger events. To these IOMs, we added the chemical dimension represented by the metallicity to help discern between different origins (similar plots were used in the past, but only to characterise metal-poor and metal-rich GCs, see for instance Posti and Helmi 2019; Woody and Schlaufman

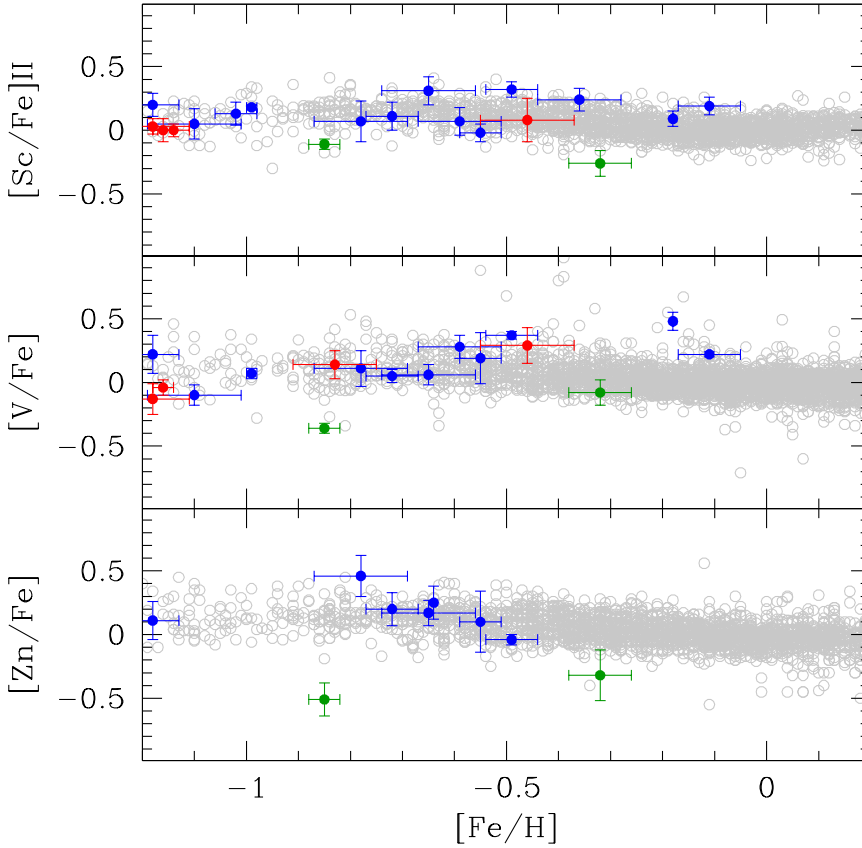


Fig. 4. Mean abundance ratios $[\text{Sc}/\text{Fe}]$, $[\text{V}/\text{Fe}]$, and $[\text{Zn}/\text{Fe}]$ for metal-rich GCs in the literature (blue filled circles are for GCs of the main progenitor, either M-B or M-D; green circles are for Sagittarius GCs, and red circles are for all other accreted GCs of the L-E, H-E, H99, GSE, and SEQ groups) compared to the field star distributions. Abundances for GCs are from Carretta (2015), Carretta et al. (2004, 2011), Cohen (2004), Crestani et al. (2019), Feltzing et al. (2009), Gratton et al. (2006, 2007), Ivans et al. (1999), Massari et al. (2017), Monaco et al. (2018), Muñoz et al. (2017, 2018, 2020), Mura-Guzmán et al. (2018), O’Connell et al. (2011), Puls et al. (2018), Ramírez and Cohen (2002), Sakari et al. (2011), Sbordone et al. (2007), and Yong et al. (2014).

2021). In each panel in Fig. 2, GCs with a common origin according to Massari et al. (2019) are marked as filled circles, corresponding to the group labelled inside the panel (see the figure caption for identifications).

The broad anti-correlation depicted in Fig. 2, with high energy GCs being less metal-rich, on average, can be explained by the tendency of more highly bound GCs being found in the inner central regions of the Galaxy, in particular in the bulge where more metal-rich GCs are preferentially located. GCs with lower binding energies are preferentially confined to lower metallicities.

Using Fig. 2 together with the guidelines from the dynamical analysis by Massari et al. (2019), it is easy to recognise that NGC 6388 is more likely compatible with the main bulge component defined by Massari et al. Its location in this plane also makes NGC 6388 incompatible with any of the accretion events known so far, also including those without a well-identified progenitor, such as the high energy (H-E) GCs.

In particular, NGC 6388 (as well as NGC 6441) seems to be barely compatible with the group of GCs with a low orbital energy which have an unknown origin in Massari et al. (2019) and that are tentatively identified with Kraken (Kruijssen et al. 2019) or Koala (Forbes 2020). This is hardly surprising since the L-E group has orbital energies very similar to those of main progenitor GCs, so that L-E GCs can be recognised as accreted objects only because they neatly lie on the accretion branch in the bifurcated age-metallicity relation (AMR; e.g. Forbes and

Bridges 2010, Leaman et al. 2013) of MW GCs. A large dispersion in metallicity (shown in Fig. 2) and a high age normalisation (shown in Massari et al. 2019) would suggest the existence of a putative massive candidate progenitor whose debris are still unidentified so far. We, however, disagree with the association of NGC 6388 to the L-E group because the location of the cluster is only marginally compatible with them, whereas it is indistinguishable from other GCs that formed in situ in the bulge of the main progenitor (panel (a) of Fig. 2). Hence we confirm the attribution of Massari et al. (2019) and Forbes (2020).

To support the view of NGC 6388 as an autochthonous GC born in our Galaxy and to exclude the tentative (yet more marginal) association we found with the L-E group definitively, we show in Fig. 3 the AMR of MW GCs, which is an additional diagnostic plot required to solve the degeneracy concerning the origin of NGC 6388. We used cluster ages for 96 GCs, with orbital parameters in Savino and Posti (2019), assembled and homogenised by Kruijssen et al. (2019). We highlight the GCs of the L-E group, NGC 6388, and NGC 6441. Massari et al. (2019) and Forbes (2020) used a simple leaky box chemical evolution model to successfully reproduce the AMR of groups of GCs with a common origin. However, the location of NGC 6388 and NGC 6441 in Fig. 3 implies that a unique simple model cannot pass through these two GCs and simultaneously through the group of L-E GCs.

By coupling Fig. 2 and Fig. 3, we conclude that the apparent closeness of NGC 6388 to the L-E GCs in the chemodynamical plane E versus $[\text{Fe}/\text{H}]$ is misleading. These plots not only confirm the assignment of NGC 6388 to the M-B group, but they may indicate that NGC 6441 could have also been erroneously assigned to the L-E group, within which it seems to occupy a similarly marginal position in panel (e) in Fig. 2.

In Appendix B, we exploit this set of diagnostic plots to discuss some extant uncertainties in the assignment of GCs to possible past accretion events. We start from Massari et al. (2019) and Forbes (2020) and are able to solve at least some of the discrepancies; of course, this will need to be revisited when more advanced releases of Gaia data are available.

Concerning the chemistry of iron-peak elements as a new criterium for selecting possible accreted GCs, we perused the literature for abundances of Sc, V, and Zn in metal-rich GCs. Mean values are plotted in the three panels of Fig. 4. The only GCs with abundance ratios of these species evidently below the distribution of Galactic stars are Pal 12 (at $[\text{Fe}/\text{H}] = -0.82$ dex) and Terzan 7 (at $[\text{Fe}/\text{H}] = -0.32$ dex; green points), which are both associated to Sag. The set of chemical tools (Sc, V, and Zn) individuated by M21a,b seems to be rather efficient in selecting Sag GCs, due to the peculiar low abundances of these elements in this dwarf galaxy (e.g. Sbordone et al. 2007).

The use of iron-peak elements for picking up accreted GCs seems to be less evident, in general, and not yet fully proven. The GCs assigned to other accreted components (red points in Fig. 4) do not seem to have lower abundances than MW stars. Moreover, when examining mean values of $[\text{Sc}/\text{Fe}]$ (the most commonly studied element among Sc, V, and Zn in GCs) collected for a large sample of GCs of any metal abundance in Carretta and Bragaglia (2021b), we again found that the average abundances of accreted GCs – apart from a couple of exceptions – are a perfect match to the MW pattern down to $[\text{Fe}/\text{H}] \sim -2.5$ dex.

The efficiency of the method proposed by M21a,b should be tested on a larger sample of GCs, to be analysed homogeneously to the comparison sample. This is something the large spectroscopic surveys in the optical range, such as WEAVE (Dalton et al. 2020) and 4MOST (de Jong et al. 2019), will efficiently provide in the near future.

Acknowledgements. We are grateful to Alessandro Savino and Davide Massari for sharing their tables of orbital parameters. This research has made use of the services of the ESO Science Archive Facility, of the SIMBAD database (Wenger et al. 2000), operated at CDS, Strasbourg, France, and in particular of the VizieR catalogue access tool (Ochsenbein et al. 2000). This research has made use of NASA's Astrophysical Data System.

References

- Adibekyan, V.Zh., Sousa, S.G., Santos, N.C. et al. 2012, *A&A*, 545, A32
- Battistini, C., Bensby, T. 2015, *A&A*, 577, A9
- Bensby, T., Feltzing, S., Lundström, I., Ilyin, I. 2005, *A&A*, 433, 185
- Bensby, T., Feltzing, S., Oey, M.S. 2014, *A&A*, 562, A71
- Bensby, T., Feltzing, S., Gould, A. et al. 2017, *A&A*, 605, A89
- Biémont, E., Godefroid, M. 1980, *A&A*, 84, 361
- Bihain, G., Israelian, G., Rebolo, R., Bonifacio, P., Molaro, P. 2004, *A&A*, A423, 777
- Brewer, J.M., Fischer, D.A., Valenti, J.A., Piskunov, N. 2016, *ApJS*, 225, 32
- Carretta, E. 2015, *ApJ*, 810, 148
- Carretta, E., Bragaglia, A. 2018, *A614*, A109
- Carretta, E., Bragaglia, A. 2019, *A&A*, 627, L7
- Carretta, E., Bragaglia, A. 2021a, arXiv:2111.12721
- Carretta, E., Bragaglia, A. 2021b, *A&A*, 646, A9
- Carretta, E., Gratton, R.G., Bragaglia, A., Bonifacio, P., Pasquini, L. 2004, *A&A*, 416, 925
- Carretta, E., Bragaglia, A., Gratton, R.G. et al. 2006, *A&A*, 450, 523
- Carretta, E., Bragaglia, A., Gratton, R.G., Lucatello, S. 2009a, *A&A*, 505, 139
- Carretta, E., Bragaglia, A., Gratton, R.G. et al. 2009b, *A&A*, 505, 117
- Carretta, E., Bragaglia, A., Gratton, R.G., D'Orazi, V., Lucatello, S. 2009c, *A&A*, 508, 695
- Carretta, E., Bragaglia, A., Gratton, R.G. et al. 2010a, *A&A*, 516, 55
- Cohen, J.G. 2004, *AJ*, 127, 1545
- Crestani, J., Alves-Brito, A., Bono, G., Puls, A.A., Alonso-García, J. 2019, *MNRAS*, 487, 5463
- Dalton, G., Trager, S., Abrams, D.C. et al. 2020, *SPIE*, 11447, 14
- da Silva, C.R., Barbuy, B., Friaça, A.C.S. et al. 2018, *A&A*, 614, A149
- de Jong, R.S., Agertz, O., Berbel, A.A. et al. 2019, *Msngr*, 175, 3
- Delgado-Mena, E., Tsantaki, M., Adibekyan, V.Zh. et al. 2017, *A&A*, 606, A94
- Feltzing, S., Primas, F., Johnson, R.A. 2009, *A&A*, 493, 913
- Feuillet, D.K., Sahlholdt, C.L., Feltzing, S., et al. 2021, *MNRAS*, 508, 1489
- Forbes, D.A. 2020, *MNRAS*, 493, 847
- Forbes, J.M., Bridges, T. 2010, *MNRAS*, 404, 1203
- Freeman, K., Bland-Hawthorn, J. 2002, *ARA&A*, 40, 487
- Gratton, R.G., Carretta, E., Claudi, R., Lucatello, S., Barbieri, M. 2003, *A&A*, 404, 187
- Gratton, R.G., Lucatello, S., Bragaglia, A. et al. 2007, *A&A*, 464, 953
- Gratton, R.G., Lucatello, S., Bragaglia, A. et al. 2006, *A&A*, 455, 271
- Gratton, R.G., Bragaglia, A., Carretta, E. et al. 2019, *A&ARv*, 27, 8
- Grevesse, N., Sauval, A.J. 1998, *SSRv*, 85, 161
- Griffith, E., Weinberg, D.H., Johnson, J.A. et al. 2021, *ApJ*, 909, 77
- Harris, W. E. 1996, *AJ*, 112, 1487
- Hasselquist, S., Carlin, J.L., Holtzman, J.A. et al. 2019, *ApJ*, 872, 58
- Horta, D., Schiavon, R.P., Mackereth, J.T. et al. 2020, *MNRAS*, 493, 3363
- Ishigaki, M.N., Chiba, M., Aoki, W. 2012, *ApJ*, 753, 64
- Ishigaki, M.N., Aoki, W., Chiba, M. 2013, *ApJ*, 771, 67
- Ivans, I.I., Sneden, C., Kraft, R.P. et al. 1999, *AJ*, 118, 1273
- Kruijssen, J.M.D., Pfeffer, J.L., Reina-Campos, M., Crain, R.A., Bastian, N. 2019, *MNRAS*, 486, 3180
- Leaman, R., VandenBerg, D.A., Mendel, J.T. 2013, *MNRAS*, 436, 122
- Lomaeva, M., Jönsson, H., Ryde, N., Schulteis, M., Thorsbro, B. 2019, *A&A*, 625, A141
- Lucey, M., Hawkins, K., Ness, M. et al. 2019, *MNRAS*, 488, 2283
- Massari, D., Koppelman, H.H., Halmi, A. 2019, *A&A*, 630, L4
- Massari, D., Mucciarelli, A., Dalessandro, E. et al. 2017, *MNRAS*, 468, 1249
- Mészáros, S., Masseron, T., García-Hernández, D.A. et al. 2020, *MNRAS*, 492, 1641
- Minelli, A., Mucciarelli, A., Romano, D. et al. 2021a, *ApJ*, 910, 114 (M21a)
- Minelli, Mucciarelli, A., Massari, D. et al. 2021b, *ApJ*, 918, L32 (M21b)

Monaco, L., Villanova, S., Carraro, G., Mucciarelli, A., Moni Bidin, C. 2018, *A&A*, 616, A181

Muñoz, C., Villanova, S., Geisler, D. 2017, *A&A*, 605, A12

Muñoz, C., Geisler, D., Villanova, S. et al. 2018, *A&A*, 620, A96

Muñoz, C., Villanova, S., Geisler, D. et al. 2020, *MNRAS*, 492, 3742

Mura-Guzmán, A., Villanova, S., Muñoz, C., Tang, B. 2018, *MNRAS*, 474, 4541

Myeong, G.C., Vasiliev, E., Iorio, G., Evans, N.W., Belokurov, V. 2019, *MNRAS*, 488, 1235

Nissen, P.E., Schuster, W.J. 2010, *A&A*, 511, L10

Nissen, P.E., Schuster, W.J. 2011, *A&A*, 530, A15

Ochsenbein, F., Bauer, P., Marcout, J. 2000, *A&AS*, 143, 23

O’Connell, J.E., Johnson, C.I., Pilachowski, C.A., Burks, G. 2011, *PASP*, 123, 1139

Posti, L., Helmi, A. 2019, *A&A*, 621, A56

Puls, A.A., Alves-Brito, A., Campos, F., Dias, B., Barbuy, B. 2018, *MNRAS*, 476, 690

Ramírez, S., Cohen, J.G. 2002, *AJ*, 123, 3277

Reddy, B.E., Tomkin, J., Lambert, D.L., Allende Prieto, C. 2003, *MNRAS*, 340, 304

Reddy, B.E., Lambert, D.L., Allende Prieto, C. 2006, *MNRAS*, 367, 1329

Roederer, I.U., Lawler, J.E. 2012, *ApJ*, 750, 76

Sakari, C.M., Venn, K.A., Irwin, M. et al. 2011, *ApJ*, 740, 106

Sbordone, L., Bonifacio, P., Buonanno, R. et al. 2007, *A&A*, 465, 815

Savino, A., Posti, L. 2019, *A&A*, 624, L9

Wenger, M., Ochsenbein, F., Egret, D. et al. 2000, *A&AS*, 143, 9

Woody, T., and Schlaufman, K.C. 2021, *AJ*, 162, 42

Yong, D., Alves Brito, A., Da Costa, G.S. et al. 2014, *MNRAS*, 439, 2638

Appendix A: Comparison with M21b for Zn

The four stars analysed in NGC 6388 by M21b were also studied in Carretta et al. (2007) and homogeneously re-analysed in Carretta and Bragaglia (2018). Here we show a detailed comparison of the Zn abundances in M21b; since they are only based on one line, Zn I 4810.54 Å is used in both studies.

In Table A.1 we list the atmospheric parameters and abundances from M21b and from our analysis. The different sets of adopted solar reference abundances imply that offsets of -0.04 dex and $+0.05$ dex for Fe and Zn, respectively, should be applied to abundances in M21b to bring their values onto our scale. In addition, an offset of $+0.08$ dex and $+0.07$ dex for Sc and V, respectively, would bring the abundances of Sc and V in M21b onto our scale, reducing the difference from field stars.

Another relevant source of differences between ours and those of M21b is the scale of atmospheric parameters used in the abundance analysis. M21b used a semi-spectroscopic set, while our method is entirely based on a photometric approach (see Carretta and Bragaglia 2018, 2021a). As an example, for the four stars under scrutiny, the effective temperatures in M21b are higher on average by ~ 88 K, with an rms scatter of 11 K.

In Table A.2 we report the sensitivities of Fe and Zn abundances to variations in the atmospheric parameters from Carretta and Bragaglia (2018). We used these sensitivities, together with the observed differences in the atmospheric parameters from Table A.1, to compute the average offset required to

bring the $[Zn/Fe]$ abundances by M21b onto our scale of atmospheric parameters. The offset turns out to be $+0.043$ dex.

Finally, also considering the difference in the adopted oscillator strength for the Zn line (-0.15 in M21b from Roederer and Lawler 2012; and -0.17 in our analysis, from Biémont and Godefroid 1980), the Zn average abundance by M21b would be on our scale $[Zn/Fe] = -0.12 + 0.05 + 0.043 + 0.02 = -0.008$ dex, which is in good agreement with our mean value -0.02 dex.

Table A.1. Comparison of our study with M21b for four stars in NGC 6388.

star	T_{eff}	$\log g$	$[Fe/H]$	v_t	$[Zn/Fe]$	T_{eff}	$\log g$	$[Fe/H]$	v_t	$[Zn/Fe]$
	M21b					us				
u63a	4100	1.33	-0.49	1.60	-0.07	4018	1.37	-0.407	1.66	+0.323
u63b	4150	1.42	-0.46	1.50	-0.21	4046	1.42	-0.415	1.75	-0.066
u63e	4000	1.16	-0.51	1.50	-0.12	3913	1.15	-0.457	1.65	+0.173
u63f	4000	1.16	-0.50	1.50	-0.07	3922	1.17	-0.414	1.57	+0.041

Solar reference abundances: M21b: Fe 7.50 and Zn 4.60 are from Grevesse and Sauval (1998). For our study: Fe 7.54 and Zn 4.59 are from Gratton et al. (2003)

Table A.2. Sensitivities of abundance ratios to variations in the atmospheric parameters for Fe and Zn.

Element	T_{eff} (K)	$\log g$ (dex)	$[A/H]$ (dex)	v_t kms $^{-1}$
Variation	50	0.20	0.10	0.10
$[Fe/H]_i$	-0.006	+0.040	+0.024	-0.045
$[Zn/Fe]_i$	-0.033	+0.011	0.000	-0.011

Appendix B: GCs with an uncertain attribution in Massari et al. (2019)

There are a few uncertainties in the association of GCs to coherent groups or components sharing the same origin in Massari et al. (2019, Ma19 in this appendix), that is the paper we used as a reference here. The attribution of some GCs was considered unsure and indicated by a question mark or there were multiple options in their Table 1. Some of these cases were discussed by Forbes (2020, F20 in this appendix), for whom the more extended set of ages in Kruijssen et al. (2019, K19 in this appendix) were available, the same we are using here. It is possible that these uncertainties will be resolved using improved kinematics based on future Gaia data releases, but in the meantime we tried to alleviate the involved degeneracy employing the chemodynamical plots E versus $[Fe/H]$ and L_z versus $[Fe/H]$, together with the AMR (whenever accurate ages are available).

Pal 2: The cluster is tagged as ‘GSE?’ in Ma19 and also F20 has the same indication. This GC is surely an accreted object, compatible with Seq, H99, and GSE (see Fig. B.1, left column);

no age is available in K19; the Lz-Fe plot shows it to be more probably of GSE origin, which is compatible with H99.

NGC 3201: The cluster is marked as 'Seq/GSE' in Ma19, while F20 puts it in the Seq sample; the uncertainty is also confirmed by the two upper plots (Fig. B.1, right column); however, the Lz-Fe plot would indicate a more probable Seq origin. Gaia DR3 and later releases are required to settle this issue.

E 3: The cluster is indicated by 'H99?' in Ma19, while F20 puts it among the in situ GCs. Looking at the upper left panel of Fig. B.2, H99 is a possibility, but also M-D; the AMR indicates a clear in situ origin and the Lz-Fe plot is in agreement, even if more marginally so. We thus agree with F20.

NGC 5139 (ω Cen:) The cluster is 'GSE/Seq' in Ma19 and Seq in F20; our plots (Fig. B.2, right column) indicate a strong preference for a GSE origin.

Rup 106: The cluster is marked as 'H99?' in Ma19 and H99 in F20; the attribution seems to be confirmed by the plots in Fig. B.3 (left column).

Pal 5: The cluster is 'H99?' in Ma19 and H99 in F20; the attribution seems clear from the Lz-Fe plot in Fig. B.3 (right column).

NGC 5634: The cluster is 'H99/GSE' in Ma19 and H99 in F20; looking at the three plots in Fig. B.4 (left column), the ambiguity in attribution still seems unresolved.

NGC 5904: The cluster is 'H99/GSE' in Ma19 and H99 in F20; also in this case, the three plots in Fig. B.4 (right column) are not resolute, although a slight preference for GSE seems possible from the Lz-Fe plane.

NGC 6101: The cluster is 'Seq/GSE' in Ma19 and Seq in F20; while both can be possible, as can be seen from Fig. B.5 (left panels), a rather strong preference for Seq is visible in the bottom plot.

Pal 15: The cluster is 'GSE?' in Ma19 and GSE in F20; the two upper panels of Fig. B.5 would also allow a Sag origin, while the lower panel seems to suggest that GSE is favoured.

NGC 6535: The cluster is 'L-E/Seq' in Ma19 and Seq in F20; the three plots on the left in Fig. B.6 leave no doubts as to a L-E origin for this GC.

Liller 1: The cluster was not attributed to any group in Ma19, while F20 gives it an in situ origin. We agree with the latter (see Fig. B.6, right panels), with a M-B origin for this GC.

NGC 6426: The cluster was attributed to the H-E group both by Ma19 and F20; however, the plots in Fig. B.7 seem to put this into question, favouring a possible H99 origin.

List of Objects

'NGC 6388' on page 1
 'NGC 5927' on page 1
 'NGC 6496' on page 1
 'NGC 6441' on page 1
 'Pal 12' on page 6
 'Terzan 7' on page 6
 'Pal 2' on page 7
 'NGC 3201' on page 8
 'E 3' on page 8
 'NGC 5139' on page 8
 'Rup 106' on page 8
 'Pal 5' on page 8
 'NGC 5634' on page 8
 'NGC 5904' on page 8
 'NGC 6101' on page 8
 'Pal 15' on page 8
 'NGC 6535' on page 8
 'Liller 1' on page 8
 'NGC 6426' on page 8

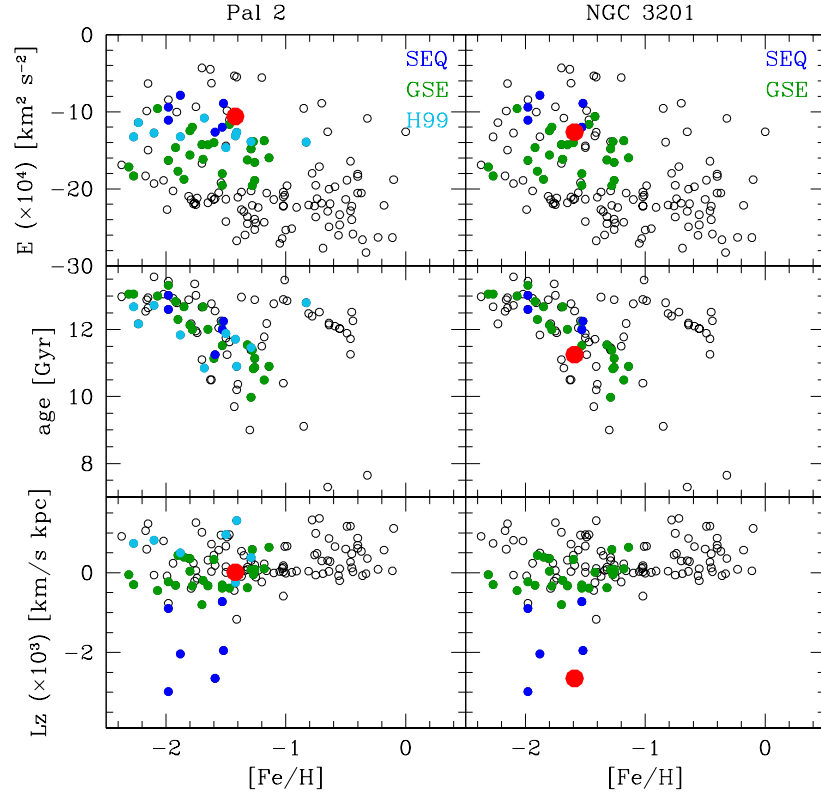


Fig. B.1. Diagnostic chemo-dynamical plots (upper and lower panels) and AMR (middle panel) for two GCs (Pal 2 and NGC 3201) with an uncertain attribution to different groups in Ma19 and F20.

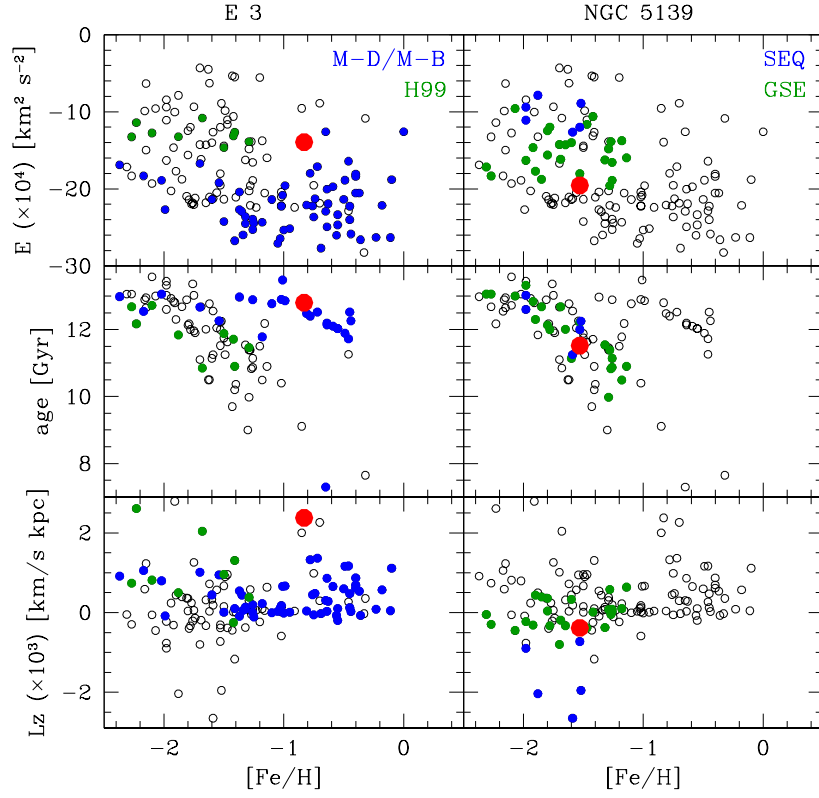


Fig. B.2. Same as Fig. B.1, but for E3 and NGC 5139 (ω Cen).

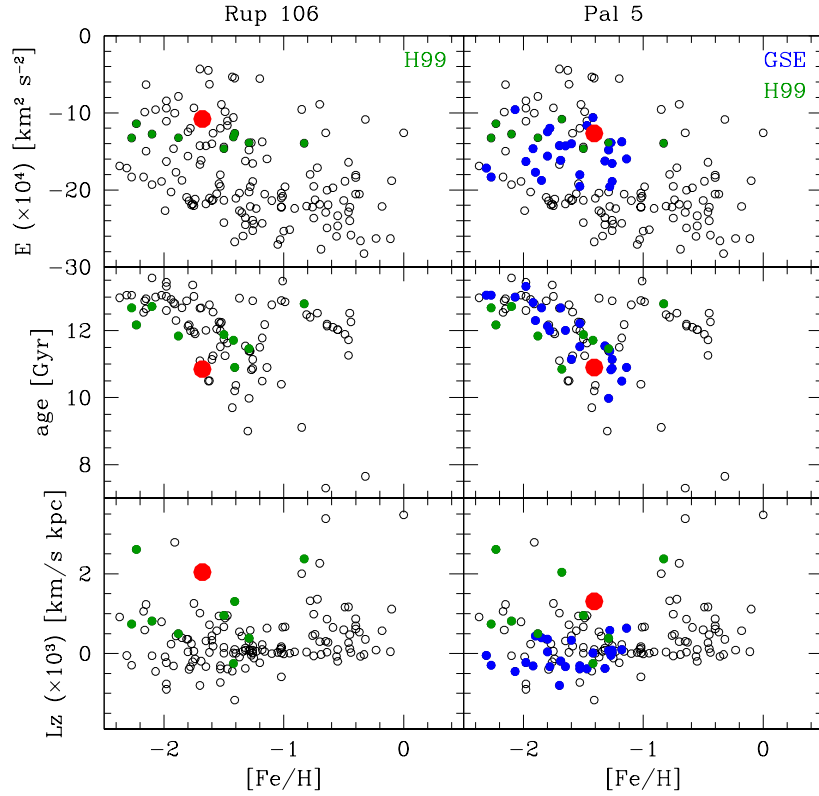


Fig. B.3. Same as Fig. B.1, but for Rup 106 and Pal 5.

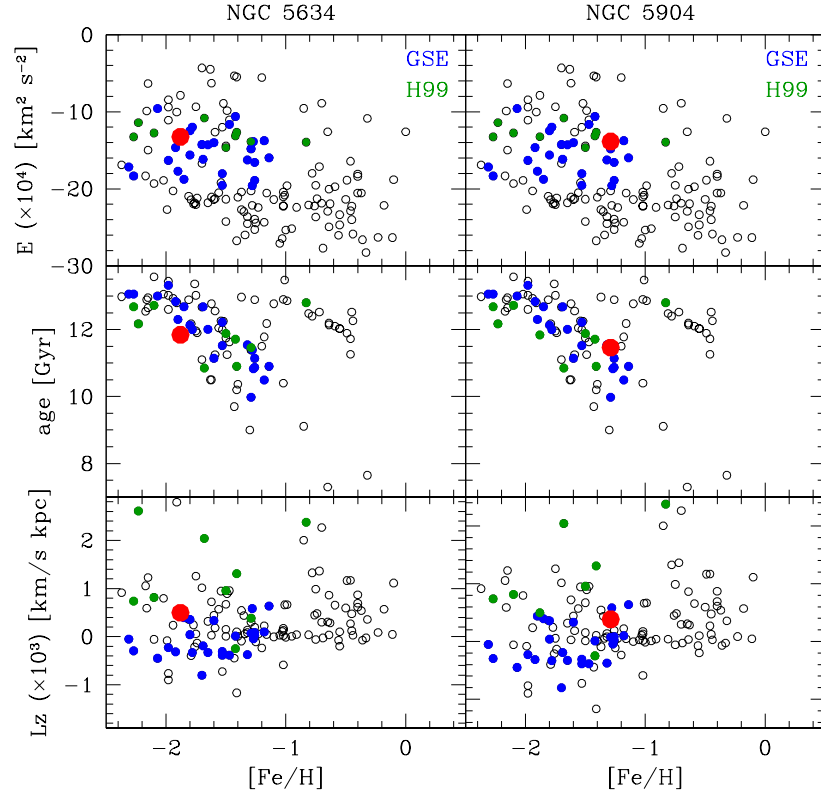


Fig. B.4. Same as Fig. B.1, but for NGC 5634 and NGC 5904.

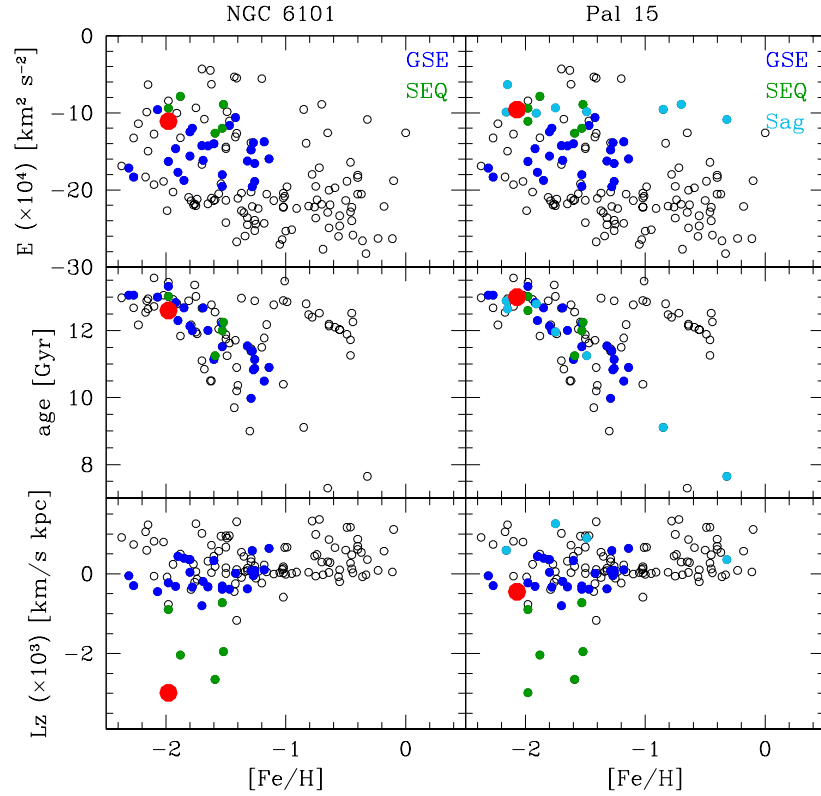


Fig. B.5. Same as Fig. B.1, but for NGC 6101 and Pal 15.

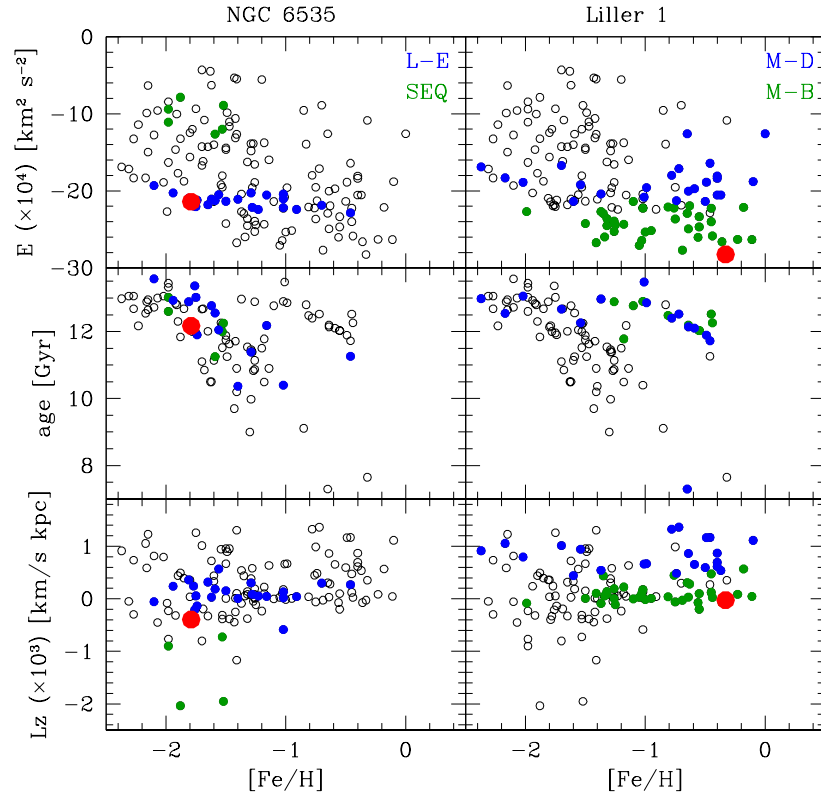


Fig. B.6. Same as Fig. B.1, but for NGC 6535 and Liller 1.

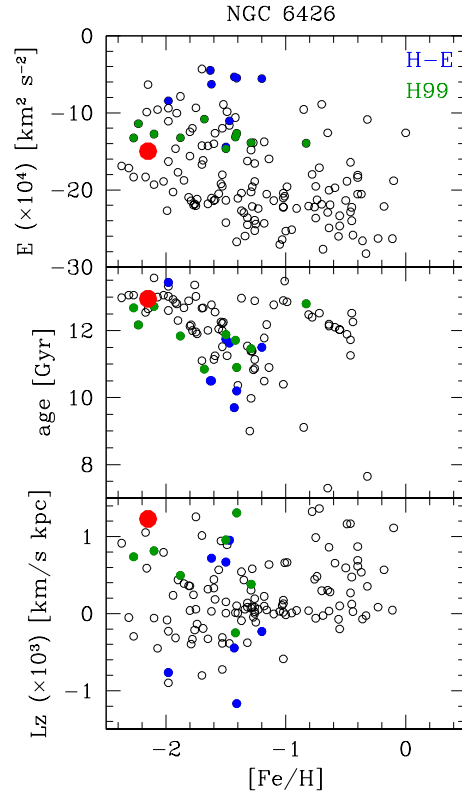


Fig. B.7. Same as Fig. B.1, but for NGC 6426.